



Preparation of Mo(Si,Al)₂ feedstock used for air plasma spraying

Hui-dong HOU^{1,2}, Xian-jin NING¹, Quan-sheng WANG¹, Bin GAO¹, Yan-bo LIU¹, Ying LIU¹

1. School of Materials Science and Engineering, Beijing Institute of Technology, Beijing 100081, China;
2. Energy, Plasma, and Electrochemistry Research Center (CREPE), Chemical and Biotechnical Engineering Department, Université de Sherbrooke, Sherbrooke J1K 2R1, QC, Canada

Received 26 October 2015; accepted 28 June 2016

Abstract: In order to prepare high quality Mo(Si,Al)₂ feedstock characterized with C40 phase, higher Al doping amount and excellent flowability, Mo(Si_{1-x},Al_x)₂ with different Al contents ($x=0, 0.1, 0.2, 0.3, 0.4, 0.5$) were synthesized by self-propagating high-temperature synthesis first and Mo(Si_{0.6},Al_{0.4})₂ was confirmed as the suitable material through X-ray diffraction analysis. A series of tests with different parameters of induction plasma spheroidization were applied to improving the flowability of feedstock. Mo(Si,Al)₂ feedstock with excellent flowability (26.2 s/50 g) was prepared through adding hydrogen into sheath gas and decreasing the powder feeding rate. The composition segregation occurred in the spheroidized powder after Al consumption and oxidation. The inhomogeneous structure of the same particle was caused by the asymmetric heating and cooling when particle passed through the plasma jet.

Key words: Mo(Si, Al)₂; C40 phase; self-propagating high-temperature synthesis; induction plasma spheroidization; composition segregation

1 Introduction

Molybdenum disilicide (MoSi₂) is an attractive coating material used in an oxidative atmosphere at high temperature due to the formation of an adherent and continuous SiO₂ film on its surface, which protects the material from further oxidation [1–3]. Whereas, there are several detrimental habits of MoSi₂ coating including the low ductility at ambient temperature, the pest oxidation in the intermediate temperature range, the evaporation of protective SiO₂ scale and the scale deterioration in the atmosphere containing water-vapor [4–6]. The former researches indicated that alloying additions to MoSi₂ can alter its anti-oxidation properties [7,8]. Mo(Si, Al)₂, with hexagonal C40-type structure, is one of the promising candidates for oxidation-resistance coating material. This material exhibits a good oxidation resistance at high temperatures over 1200 °C providing a continuous alumina scale and an Al–Si–O film at lower temperatures [9]. Besides, Al₂O₃ has proved to be effective for adjusting viscosity and improving the crystallization temperature of SiO₂ [10]. Therefore,

Mo(Si, Al)₂ is considered to have definite advantages over MoSi₂ for oxidation-resistance coating at service temperatures up to 1400 °C [11].

Depending on Al contents, Mo(Si, Al)₂ possesses different crystal structures (C11_b, C40, C54) which show different oxidation behaviors and mechanisms [5,12]. Little discrepancy concerning critical value of crystal transformation occurs between the theory and experiment [13,14]. The Mo(Si, Al)₂ synthesis methods and operating condition may influence this critical value. In order to synthesize Mo(Si, Al)₂ with pure crystal structure, it is essential to clarify primarily the critical value of synthesis method and operating condition used in this work. Besides, although different preparation methods were applied to fabricating MoSi₂-based coatings, such as supersonic plasma spraying [15], high velocity oxygen fuel spraying (HVOF) [16], electrothermal explosion ultrahigh speed spraying (EEUSS) [17] and air plasma spraying (APS) [18]. Feedstocks of metals, alloys and ceramics for thermal spray applications have to meet several specifications. In order to ensure high spray efficiency and better coating properties, particle shape, size distribution, powder

flowability and density are the important factors that need to be controlled [19]. Inductively coupled plasma (ICP) with high enthalpy content has played an increasing important role in a wide range of technological processes, such as particle densification and spheroidization, plasma spray deposition of materials. It is a truism that particle spheroidisation is one of the successful applications of ICP and plays a key role in substantial improvement of powder quality and fluidity [20].

For the purpose of clarifying the critical value of Mo(Si, Al)₂ crystal transformation in self-propagating high-temperature synthesis (SHS) and obtaining Mo(Si, Al)₂ powder with pure crystal structure, a series of Mo(Si_{1-x}, Al_x)₂ powders with different Al contents ($x=0, 0.1, 0.2, 0.3, 0.4, 0.5$) were synthesized by SHS in the present work. Through optimizing the parameters of induction plasma spheroidization (IPS), Mo(Si, Al)₂ feedstock with excellent flowability and nearly pure C40 crystal structure was also prepared. The crystal transformation of Mo(Si, Al)₂ during SHS and IPS were discussed in detail.

2 Experimental

2.1 Synthesis of Mo(Si, Al)₂ powder by SHS

Commercialized Mo, Si and Al powders (Qinhuangdao Eno High-Tech Material Development Co., Ltd., China) with the grain size of $\sim 3 \mu\text{m}$ and the chemical purity of 99.9% were used as raw materials for combustion synthesis. The mole ratio of powder mixtures was chosen according to Mo(Si_{1-x}, Al_x)₂ with x range of 0–0.5. At the first step, reactant mixtures with stoichiometric ratio were well-blended, dried at 100 °C for 24 h, cold-pressed to a compact brick-like sample. Combustion reactions were initiated at one end of each sample, using electrical arc under 99.9% pure argon atmosphere with wave propagating mode (Dalian Ke Mao experimental facilities Co., Ltd., China).

2.2 Preparation of Mo(Si, Al)₂ feedstock

The SHS synthesized powder was crashed

mechanically and meshed. The coarse powder ($d_{50}=50 \mu\text{m}$) was then treated by IPS to improve the flowability and apparent density. The plasma was generated by an induction-plasma torch (Model PL 35, TEKNA Plasma Systems, Sherbrooke, Quebec, Canada) in connection with a radio frequency (R.F.) power-supply of 3 MHz. The fine powder ($d_{50}=3.9 \mu\text{m}$) was agglomerated into spherical or near-spherical particles with several tens of microns by spray drying process. The spray-dried particle may be crushed and blocked the powder feeding nozzle during APS process due to the low bonding strength of hollow agglomerated particles. Therefore, IPS process was also employed to densify the agglomerated particles. The parameters of IPS are listed in Table 1.

2.3 Characterizations

The surface morphologies and cross-sectional microstructures of powder were examined with a scanning electron microscope (SEM, Philips S-4800, Hitachi Ltd., Yoshida-Cho, Totsuka-Ku, Yokohama, Japan), which was equipped with an Oxford Inca energy dispersive spectroscopy (EDS) for chemical analysis. The phase structure of powder was analyzed by X-ray diffraction (XRD, Cu K α , X'pert PRO, PANalytical B.V., Almelo, Netherlands). The particle size distribution was measured by a laser particle size analyser (Mastersizer 2000, Malvern, British). The particle flowability was measured by a standard flowmeter (FT-102B, Ningbo Rooko instrument Co., Ltd., China).

3 Results and discussion

3.1 Characterization of SHS powder

Figure 1 shows the XRD patterns of SHS synthesized Mo(Si_{1-x}, Al_x)₂ powder with different contents of Al. Without the adding of Al ($x=0$), nearly pure tetragonal MoSi₂ (C11_b) was identified for the product. When $x=0.1$, the coexistence of C11_b and C40 phases was observed in the SHS product. In the case of $0.2 \leq x \leq 0.4$, the main phase has fully transformed to C40 phase with three weak peaks of C11_b. As the content of

Table 1 Main parameters of IPS

Test run No.	Powder	Gas flow rate/(mL·min ⁻¹)			Reactor pressure/kPa	Feeding rate/(g·min ⁻¹)	Mass balance (before/after)/g
		Central gas (Ar)	Sheath gas (Ar)	Sheath gas (H ₂)			
1	Crushed	18	70	0	75.834	75	100/80
2	Crushed	18	60	7	75.834	75	100/68
3	Crushed	18	60	7	75.834	50	100/64
4	Spray dried	18	60	7	75.834	75	100/63
5	Spray dried	18	60	7	75.834	50	100/60
6	Spray dried	18	60	7	75.834	15	100/53

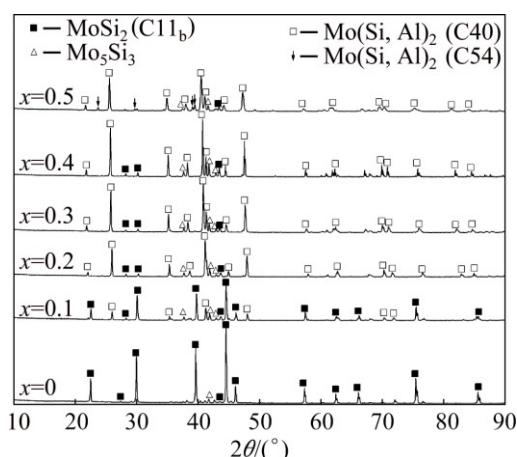


Fig. 1 XRD patterns of SHS synthesized $\text{Mo}(\text{Si}_{1-x}, \text{Al}_x)_2$ powder with different Al contents

Al reaches 0.5, C54 phase appeared in addition to C40 phase. In most products ($0.2 \leq x \leq 0.4$), trace amount of Mo_5Si_3 and MoSi_2 were identified which were most probably caused by spot segregation during SHS process. SHS is a synthetic process in which initial reactants spontaneously transform into products due to the exothermic heat of reaction. Once the reactants are ignited, a combustion wave is established across the entire sample to complete the reaction [21]. It was reported that any increase in Al addition up to $x=0.15$ will increase the combustion temperature, whereas the combustion temperature decreases as the Al content exceeds 0.15 [22]. This behavior can be attributed to the eutectic formation of Al–Si which can spread among the solid reactants and facilitate the combustion reaction by increasing thermal conductivity as well as diffusion rate and make the exothermic reaction more violent. However, the amount of latent heat required to form Al–Si liquid is supplied by the heat generated in combustion front. The large amount of Al–Si liquid caused by higher Al content absorbs much more heat in combustion front and decreases the combustion temperature of the Mo–Si–Al system. It was reported that the SHS reaction can take place spontaneously only when the adiabatic temperature (T_{ad}) is higher than 1800 K [23]. This means that the combustion temperature of Mo–Si–Al should be higher than T_{ad} (1800 K) and then the reaction system can be self-sustained. Since a large amount of Al–Si liquid absorbs much heat and even decreases the combustion temperature lower than 1800 K, the reaction will stop. In this work, conventional SHS facility is without preheating equipment, so, the reaction system cannot be self-sustained when Al content exceeds 0.5. This fact showed that large amount of Al–Si liquid even terminate the SHS reaction. Therefore, pure $\text{Mo}(\text{Si}, \text{Al})_2$ with C54 structure cannot be synthesized by traditional SHS facility.

Compared with C11_b phase, it is proposed that C40 phase with higher symmetry performs less brittle [24]. Besides, $\text{Mo}(\text{Si}_{1-x}, \text{Al}_x)_2$ with C40 phase can be formed with fairly wide Al content range and a quite narrow Mo content of about 33.3% (mole fraction) according to Mo–Si–Al ternary phase diagram at 1550 °C in Fig. 2 [13]. This characteristic of wide content range of Al makes it possible to synthesize C40 structured $\text{Mo}(\text{Si}, \text{Al})_2$ and avoid the appearance of brittle phase C11_b. In order to obtain large amount of C40 phase with higher Al doping, the molar ratio of Mo to Si to Al powder was kept to be 33.3: 40.0: 26.7 (corresponding compositions were marked with dotted lines in Fig. 2). This molar ratio was identical with the stoichiometric ratio of $\text{Mo}(\text{Si}_{0.6}, \text{Al}_{0.4})_2$.

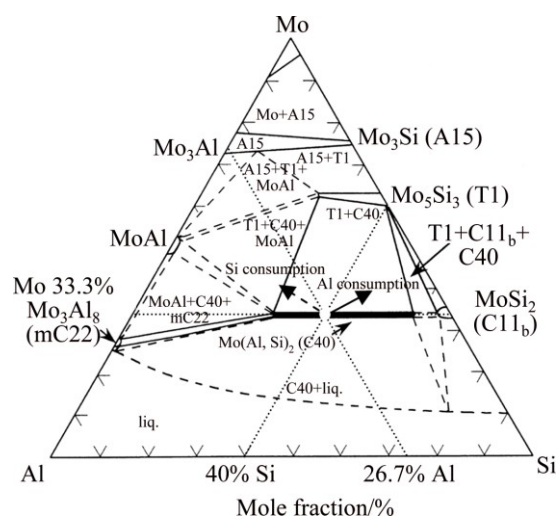


Fig. 2 Mo–Si–Al ternary phase diagram at 1550 °C [13]

3.2 Characterization of IPS powder

Figure 3 shows the morphologies of the coarse powder crushed and the spheroidized powder treated by different IPS parameters of No.1, No. 2 and No. 3. Before IPS treatment, the crushed particles present porous irregular shape and clumped distribution. After IPS process without adding hydrogen to sheath gas (No. 1), no spheroidization can be observed (Fig. 3(b)). Nevertheless, an obvious change occurred when hydrogen gas (10.3%, volume fraction) was added to sheath gas (No. 2). Small size particles show quasi-spherical morphology although the coarser particles remain the irregular shape (Fig. 3(c)). Since monatomic argon ionization can provide less energy during the plasma sustaining, as the adding of diatomic hydrogen gas can improve the enthalpy of plasma dramatically by two step transformation (dissociation and ionization) from gas to plasma. The morphologies in Figs. 3(b) and (c) clarify that addition of hydrogen increased the enthalpy of plasma significantly and improved the heating and spheroidization in this study. When powder is sent into the core of induction plasma jet, the heat

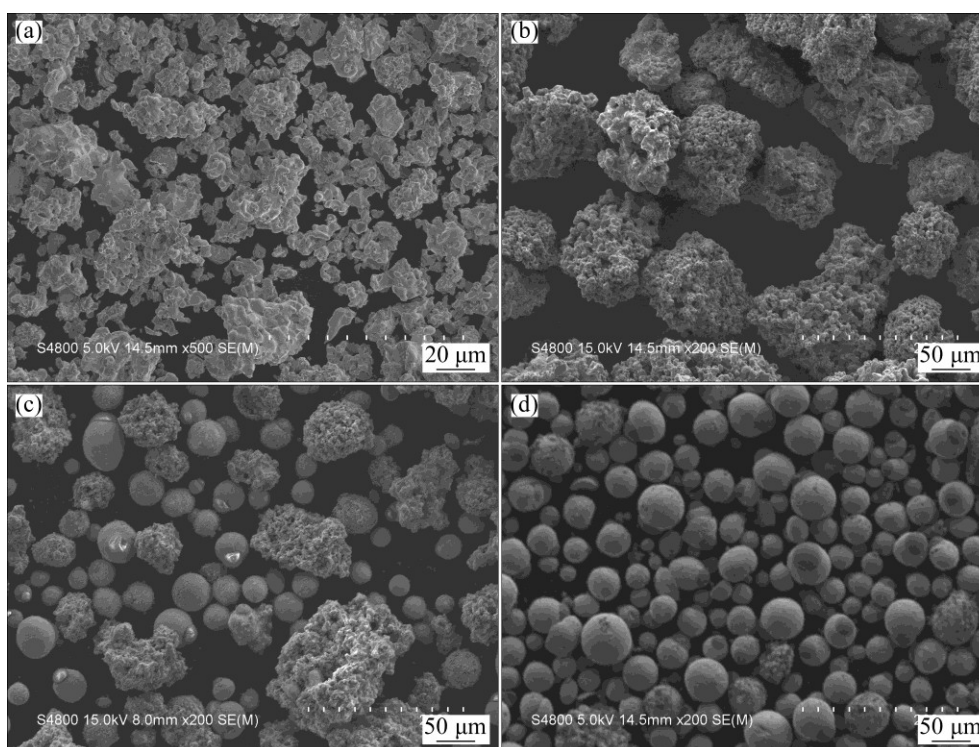


Fig. 3 Morphologies of coarse powder (a) and spheroidized powder treated by IPS technological parameter of No.1 (b), No.2 (c) and No. 3 (d)

transfer of particle surface involves the conduction and convection from plasma and the radiation and evaporation heat losses from particle. Since the radiation energy losses from particle surface to the surrounding increases, the heating and melting of particle become more difficult for the particles with larger diameter [20]. This was further confirmed by the un-melted irregular shape for the coarser particles after IPS process (Fig. 3(c)).

After decreasing feeding rate from 75 g/min of No. 2 parameter to 50 g/min of No. 3 parameter, almost all the particles show quasi-spherical morphology which indicates that the particles experienced a sufficient molten state. It was reported that the feeding rate of powder can affect the plasma temperature significantly [25,26]. Simulated result indicates that for YSZ particles of 25 μm , the plasma temperature along the particle trajectory can decrease dramatically from 8500 K to 4000 K as the feeding rate increases from 2 to 20 g/min. On the other hand, the high melting point of $\text{Mo}(\text{Si}, \text{Al})_2$ in this study makes the effect of feeding rate more serious.

Figure 4 shows the morphologies of the spray-dried powder (Figs. 4(a) and (b)) and the spheroidized powder treated by different IPS parameters of No. 4 (Figs. 4(c) and (d)), No. 5 (Figs. 4(e) and (f)) and No. 6 (Figs. 4(g) and (h)), respectively. The spray-dried powder shows a good spherical appearance of rough surface. Each

particle comprises large amount of fine particles. These fine particles gathered loosely with sharp edges. The powder with polyporous surface and even hollow powder will re-melt and solidify into smaller, dense and solid sphere [20]. The partial evaporation of particle during plasma treatment also decreases the size of spheroidized powder [27]. Compared with the powder in Fig. 4(a), many obvious fine particles around 15 μm are shown in Figs. 4(c), (e), and (g) (pointed by arrows). This means that obvious shrinkage of particles happened during the IPS process.

Due to the high feeding rate (75 g/min) of No. 4 parameter, some small particles are close as they enter the plasma jet, which resulted in the connection and joining of particles (marked by circles in Fig. 4(c)). Unlike un-melted crushed particles (Fig. 3(c)), most agglomerate particles melted during the IPS treatment (Fig. 4(d)) although the same parameter was used for these two cases. This may be attributed to the difference of morphology and consequently heating transfer between the two powders. Compared with the particle of irregular shape, the spherical agglomerate particle has lower in-flight velocity and longer residence time in plasma jet, and then absorbs more energy. The difference between spheroidized powder of No. 5 and No. 6 lies only in the surface roughness. Powder of No. 5 (feeding rate of 50 g/min) reveals a rough surface with much plate-like flakes while powder of No. 6 (feeding rate of

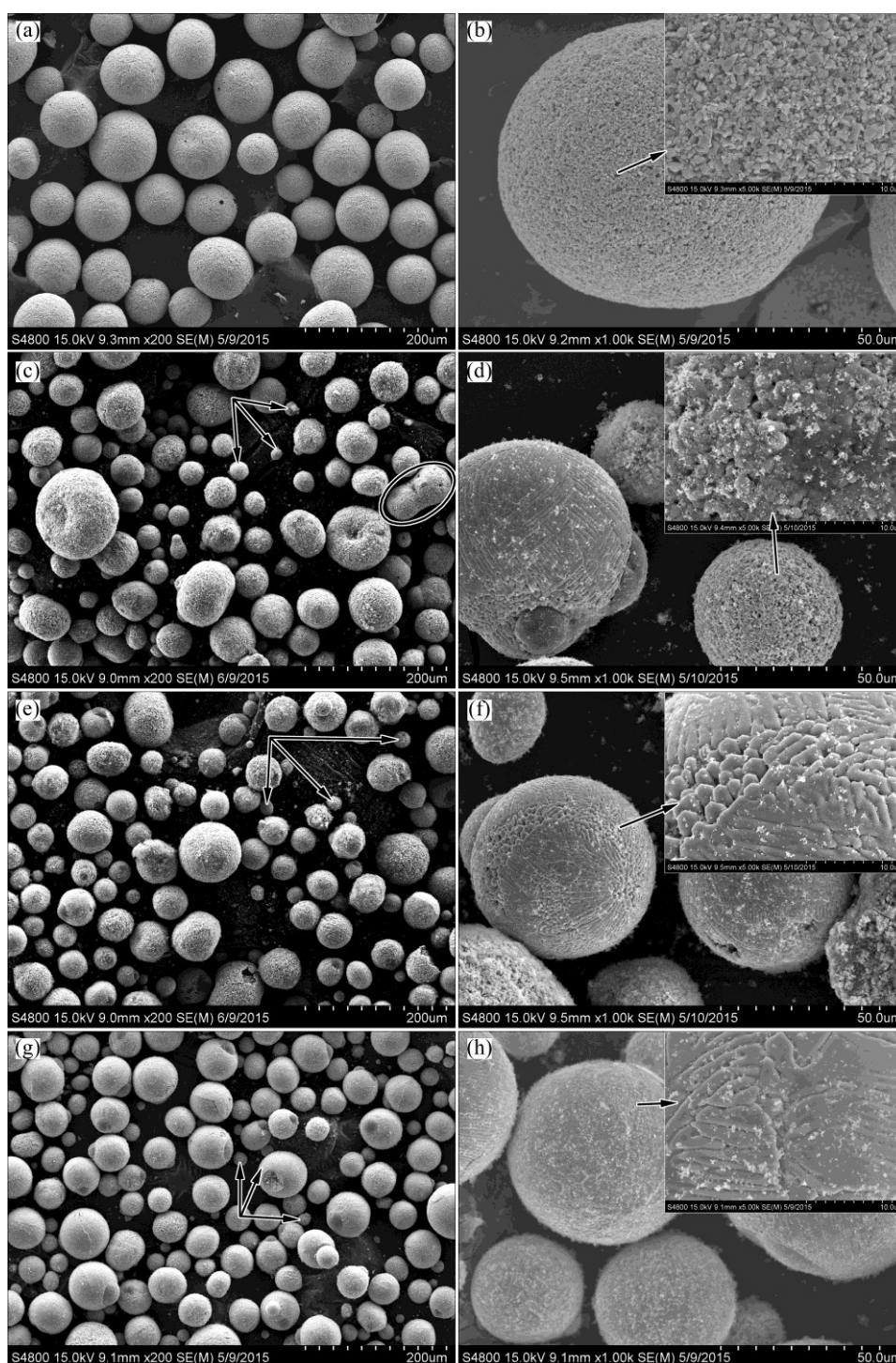


Fig. 4 Morphologies of spray-dried powder (a, b) and spheroidized powder treated by different IPS parameters of No. 4 (c, d), No. 5 (e, f) and No. 6 (g, h)

15 g/min) shows a relative smooth one. The powder treated by No. 6 parameter possesses the best flowability, i.e., 26.2 s/50 g. Many fine deposits loosely adhere on the particle surface (Figs. 4(d), (f), (h)) which can be easily removed by washing the powders with alcohol solvent and ultrasonic vibration. That is because the partial evaporation of particle happened during plasma treatment and then condensed on the particle surface

nearly [28]. The evaporation phenomenon also decreases the particle size as mentioned before.

Figure 5 shows the XRD patterns of spray-dried powder before and after IPS treatment. Before IPS process, the agglomerated powder is composed mainly of $\text{Mo}(\text{Si}, \text{Al})_2$ with C40 structure and trace amount of Mo_5Si_3 and MoSi_2 , which is same as SHS product since the low treating temperature of $<300^\circ\text{C}$ used in spray

drying. The peaks of MoSi_2 near 28° and 30° become much weaker after IPS treatment. The high temperature of plasma induced the evaporation and oxidation of element Si. Most MoSi_2 transformed into Mo_5Si_3 (lower Si content than MoSi_2) after the Si depletion. Besides, the diffraction pattern becomes wider due to the fairly fast cooling rate and the powder consists of $\text{Mo}(\text{Si}, \text{Al})_2$ and Mo_5Si_3 .

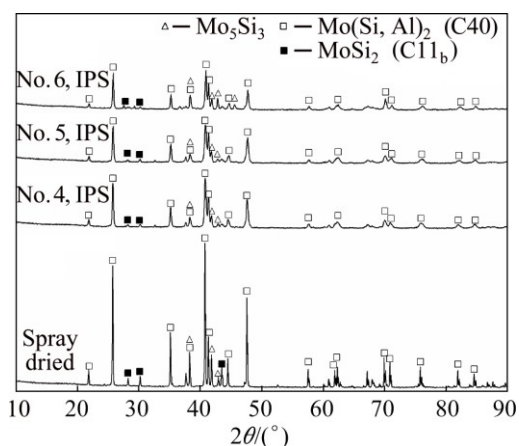


Fig. 5 XRD patterns of spray-dried powder and powder treated by different IPS parameters (No. 4, No. 5, No. 6)

Figure 6 shows the typical cross-sectional images of IPS treated powder (No. 6). As for spheroidized powder with hat-like phase (Fig. 6(a)), it was confirmed by EDS that the black hat-like phase on one side of some particle is aluminum oxide. This was induced by the trace oxygen entered plasma reactor with powder. Besides,

oxygen gas could come from the impurities in the plasma gases. It can also come from the leakage of plasma spray chamber [28]. The rest part of particle consists mainly of two phases, i.e., the grey phase and the net-like lighter one. The latter phase possesses higher Mo content as indicated by EDS line scanning. According to Mo–Si–Al ternary phase diagram (Fig. 2), the composition of $\text{Mo}(\text{Si}_{0.6}, \text{Al}_{0.4})_2$ (white point) changes along the direction of black arrow and enters the coexisting Mo_5Si_3 – $\text{Mo}(\text{Si}, \text{Al})_2$ region accompanying with the consumption of Al. Therefore, the grey phase and the lighter one are composed of $\text{Mo}(\text{Si}, \text{Al})_2$ with C40 structure and Mo_5Si_3 (higher Mo content than $\text{Mo}(\text{Si}, \text{Al})_2$), respectively. The cooling rate of molten droplet in IPS process was proved to be less than 10^4 K/s in the previous research [18], this cooling rate cannot suppress the formation of Mo_5Si_3 . It should be pointed out that the composition of *A* will also enter into the two phases region, Mo_5Si_3 – $\text{Mo}(\text{Si}, \text{Al})_2$, if Si consumes (Fig. 2).

For the spheroidized powder without hat-like aluminum oxide, some particles present an uniformly distributed Mo_5Si_3 (Fig. 6(b)) while the others present an inhomogeneous distribution with finer $\text{Mo}(\text{Si}, \text{Al})_2$ grains on the top-left side of Fig. 6(c). The crystal phase of a particle is determined by its temperature history [29]. YE et al [29] found that a spheroidized alumina particle showed α -phase and γ -phase together. The α -phase formation in alumina can be attained through a moderate cooling and nucleation history in melts, while γ -phase formation is preferred under considerably high cooling. In Stergiou's work [24], $\text{Mo}(\text{Al}, \text{Si})_2$ was arc melted and

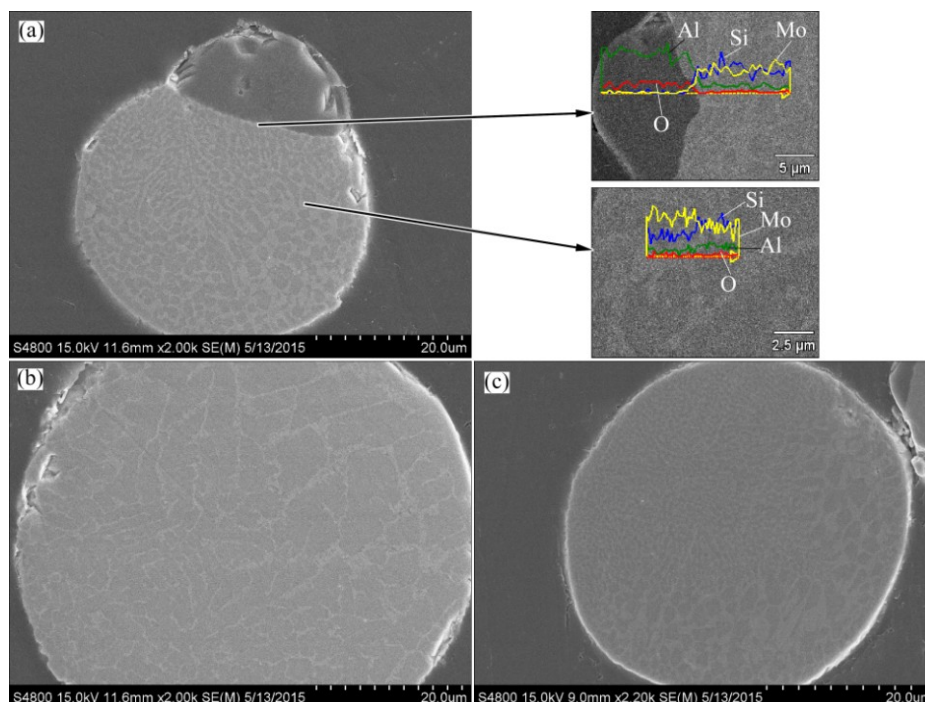


Fig. 6 Typical cross-sectional images of powder treated by IPS (No.6) with hat-like aluminum oxide (a), homogeneous distribution (b), inhomogeneous distribution (c) and EDS line scanning results

cast on a Mo wheel to fabricate a ribbon with the thickness around 50 μm . The rapidly solidified zone (wheel side) of the melt-spun ribbons showed different Mo_5Si_3 phase distributions with the opposite side. This phenomenon is similar with Fig. 6(c) in this work. The temperature and concentration field in the plasma volume are intricate. The particle trajectory and heating process are always affected by the turbulence and even the cold gas in thermal plasma stream [30]. Therefore, these inhomogeneous structures may be caused by the asymmetric heating when particle passed through the plasma jet. The different temperature fields of upwind and downwind area of particle surface performed a different solidification during the cooling stage.

4 Conclusions

1) $\text{Mo}(\text{Si},\text{Al})_2$ with nearly pure C40 structure can be designed as $\text{Mo}(\text{Si}_{0.6}, \text{Al}_{0.4})_2$ with the maximum Al content in SHS process.

2) The addition of hydrogen into sheath gas sharply increases the enthalpy of ICP. The reduced powder feeding rate facilitates the melting process of particles and gives them smooth surface after cooling.

3) The composition segregation occurs in the spheroidized powder after consumption and oxidation of Al and Si. The different sides of one particle contacting with different heating flows show different segregations and inhomogeneous phase distribution.

Acknowledgements

The authors would like to express their appreciation to Prof. Jocelyn Veilleux and Mr. Jérôme Menneveux (Energy, Plasma, and Electrochemistry Research Center (CREPE), Chemical and Biotechnical Engineering Department, Université de Sherbrooke) for giving the support of paper writing and revision.

References

- [1] FU Qian-gang, ZHANG Jia-ping, ZHANG Zheng-zhong, LI He-jun, SUN Can. SiC– MoSi_2 / ZrO_2 – MoSi_2 coating to protect C/C composites against oxidation [J]. Transactions of Nonferrous Metals Society of China, 2013, 23: 2113–2117.
- [2] ZHANG Wu-zhuang, ZENG Yi, GBOLOGAH L, XIONG Xiang, HUANG Bai-yun. Preparation and oxidation property of ZrB_2 – MoSi_2 /SiC coating on carbon/carbon composites [J]. Transactions of Nonferrous Metals Society of China, 2011, 21: 1538–1544.
- [3] INGEMARSSON L, HELLSTROM K, JOHANSSON L G, SVENSSON J E, HALVARSSON M. Oxidation behaviour of a $\text{Mo}(\text{Si}, \text{Al})_2$ based composite at 1500 °C [J]. Intermetallics, 2011, 19: 1319–1329.
- [4] HE Zi-bo, LI He-jun, SHI Xiao-hong, FU Qian-gang, WU Heng. Formation mechanism and oxidation behavior of MoSi_2 –SiC protective coating prepared by chemical vapor infiltration/reaction [J]. Transactions of Nonferrous Metals Society of China, 2013, 23: 2100–2106.
- [5] INGEMARSSON L, HELLSTROM K, CANOVIC S, JONSSON T, HALVARSSON M, JOHANSSON L G, SVENSSON J E. Oxidation behavior of a $\text{Mo}(\text{Si},\text{Al})_2$ composite at 900–1600 °C in dry air [J]. Journal of Materials Science, 2013, 48: 1511–1523.
- [6] ZHANG Yu-lei, LI He-jun, HU Zhi-xiong, LI Ke-zhi, ZHANG Lei-lei. C/SiC/ MoSi_2 –SiC–Si multilayer coating for oxidation protection of carbon/carbon composites [J]. Transactions of Nonferrous Metals Society of China, 2013, 23: 2118–2122.
- [7] YI Dan-qing, LAI Zong-he, LI Chang-hai, AKSELSEN O M, ULVENSOEN J H. Ternary alloying study of MoSi_2 [J]. Metallurgical and Materials Transactions A, 1998, 29: 119–129.
- [8] STROM E, CAO Y, YAO Y M. Low temperature oxidation of Cr-alloyed MoSi_2 [J]. Transactions of Nonferrous Metals Society of China, 2007, 17: 1282–1286.
- [9] FEI Xiao-ai, NIU Ya-ran, JI Heng, HUANG Li-ping, ZHENG Xue-bin. Oxidation behavior of Al_2O_3 reinforced MoSi_2 composite coatings fabricated by vacuum plasma spraying [J]. Ceramics International, 2010, 36: 2235–2239.
- [10] HUANG H H, LIU Y S, CHEN Y M, HUANG M C, WANG M C. Effect of oxygen pressure on the microstructure and properties of the Al_2O_3 – SiO_2 thin films deposited by E-beam evaporation [J]. Surface & Coatings Technology, 2006, 200: 3309–3313.
- [11] TABARU T, SHOBU K, SAKAMOTO M, HANADA S. Effects of substitution of Al for Si on the lattice variations and thermal expansion of $\text{Mo}(\text{Si}, \text{Al})_2$ [J]. Intermetallics, 2004, 12: 33–41.
- [12] RAMBERG C E, WORRELL W L. Oxidation kinetics and composite scale formation in the system $\text{Mo}(\text{Al}, \text{Si})_2$ [J]. Journal of the American Ceramic Society, 2002, 85: 444–452.
- [13] MARUYAMA T, YANAGIHARA K. High temperature oxidation and peeling of $\text{Mo}(\text{Si}, \text{Al})_2$ [J]. Materials Science and Engineering A, 1997, 239–240: 828–841.
- [14] TABARU T, SHOBU K, HIRAI H, HANADA S. Influences of Al content and secondary phase of $\text{Mo}_3(\text{Si}, \text{Al})_3$ on the oxidation resistance of Al-rich $\text{Mo}(\text{Si},\text{Al})_2$ -base composites [J]. Intermetallics, 2003, 11: 721–733.
- [15] WU Heng, LI He-jun, LEI Qing, FU Qian-gang, MA Chao, YAO Dong-jia, WANG Yong-jie, SUN Can, WEI Jian-feng, HAN Zhi-hai. Effect of spraying power on microstructure and bonding strength of MoSi_2 -based coatings prepared by supersonic plasma spraying [J]. Applied Surface Science, 2011, 257: 5566–5570.
- [16] REISEL G, WIELAGE B, STEINHÄUSER S, MORGENTHAL I, SCHOLL R. High temperature oxidation behavior of HVOF-sprayed unreinforced and reinforced molybdenum disilicide powders [J]. Surface & Coatings Technology, 2001, 146: 19–26.
- [17] HOU Shi-xiang, LIU Zong-de, LIU Dong-yu, LI Bao-rang, ZHANG Nai-qiang. Microstructure and oxidation resistance of Mo–Si and Mo–Si–Al alloy coatings prepared by electro-thermal explosion ultrahigh speed spraying [J]. Materials Science and Engineering A, 2009, 518: 108–117.
- [18] HOU Hui-dong, NING Xian-jin, WANG Quan-sheng, LIU Ying, LIU Yan-bo. Anti-ablation behavior of air plasma-sprayed $\text{Mo}(\text{Si}, \text{Al})_2$ coating [J]. Surface & Coatings Technology, 2015, 274: 60–67.
- [19] KUMAR S, SELVARAJAN V, PADMANABHAN P V A, SREEKUMAR K P. Spheroidization of metal and ceramic powders in thermal plasma jet: Comparison between experimental results and theoretical estimation [J]. Journal of Materials Processing Technology, 2006, 176: 87–94.
- [20] BOULOS M I. Thermal plasma processing [J]. IEEE Transactions on Plasma Science, 1991, 19: 1078–1089.
- [21] XU Jian-guang, ZHANG Hou-an, YAN Jian-hui, ZHANG Bao-lin, LI Wen-lan. Effect of argon atmosphere on the formation of MoSi_2 by self-propagating combustion method [J]. International Journal of Refractory Metals and Hard Materials, 2007, 25: 318–321.

- [22] ESMAEILI G M, SAIDI A, ABBASI M H. Lattice variations and phase evolutions during combustion reactions in Mo–Si–Al system [J]. *Journal of Alloys and Compounds*, 2009, 472: 84–90.
- [23] MOORE J J, FENG H J. Combustion synthesis of advanced materials: Part I. Reaction parameters [J]. *Progress in Materials Science*, 1995, 39: 243–273.
- [24] STERGIU A, TSAKIROPOULOS P. Study of the effects of Al, Ta, W additions on the microstructure and properties of MoSi₂ base alloys [J]. *Materials Research Society*, 1995, 364: 911–916.
- [25] PIERRE P, JAVAD M, BOULOS M I. Heating of powders in an R.F. inductively coupled plasma under dense loading conditions [J]. *Plasma Chem Plasma Process* 1987, 7: 29–52.
- [26] COLOMBO V, GHEDINI E, SANIBONDI P. Three-dimensional investigation of particle treatment in an RF thermal plasma with reaction chamber [J]. *Plasma Sources Science and Technology*, 2010, 19: 1–13.
- [27] LI Ya-li, ISHIGAKI T. Spheroidization of titanium carbide powders by induction thermal plasma processing [J]. *Journal of the American Ceramic Society*, 2001, 84: 1929–1936.
- [28] JIANG Xian-liang, BOULOS M I. Induction plasma spheroidization of tungsten and molybdenum powders [J]. *Transactions of Nonferrous Metals Society of China*, 2006, 16: 13–17.
- [29] YE R, ISHIGAKI T, JUREWICZ J, PROULX P, BOULOS M I. In-flight spheroidization of alumina powders in Ar–H₂ and Ar–N₂ induction plasmas [J]. *Plasma Chemistry and Plasma Processing*, 2004, 24: 555–571.
- [30] RAHMANE M, SOUCY G, BOULOS M I. Diffusion phenomena of a cold gas in a thermal plasma stream [J]. *Plasma Chemistry and Plasma Processing*, 1995, 16: s169–s189.

大气等离子喷涂用 Mo(Si,Al)₂ 粉末的制备

侯晖东^{1,2}, 宁先进¹, 王全胜¹, 高斌¹, 柳彦博¹, 刘颖¹

1. 北京理工大学 材料科学与工程学院, 北京 100081;

2. Energy, Plasma, and Electrochemistry Research Center (CREPE),

Chemical and Biotechnical Engineering Department, Université de Sherbrooke, Sherbrooke J1K 2R1, QC, Canada

摘要: 为了制备含有 C40 相、较高 Al 元素掺杂量以及高流动性的优质 Mo(Si, Al)₂ 喷涂粉末, 使用自蔓延燃烧合成法制备不同 Al 掺杂量的($x=0.1, 0.2, 0.3, 0.4, 0.5$) Mo(Si_{1-x}, Al_x)₂ 粉末, 通过 X 射线衍射分析确定 Mo(Si_{0.6}, Al_{0.4})₂ 为最优产物, 采用一系列不同工艺参数的感应等离子球化工艺改善粉末的流动性。通过在鞘气中加入氢气并且降低送粉率, 制备具有优异流动性能(26.2 s/50 g)的喷涂粉末 Mo(Si, Al)₂。由于 Al 的损失以及氧化, 导致球化后的粉末出现了成分偏析, 且同一颗粒中出现各向异性的成分偏析, 该现象是由于颗粒穿过等离子射流时的不均匀受热以及冷却造成。

关键词: Mo(Si, Al)₂; C40 相; 自蔓延高温合成; 感应等离子球化; 成分偏析

(Edited by Xiang-qun LI)